Skin Heating Effects of Millimeter-Wave Irradiation—Thermal Modeling Results

D. A. Nelson, M. T. Nelson, T. J. Walters, and P. A. Mason

***Abstract*—Millimeter microwaves (MMWs) are a subset of RF in the 30–300-GHz range. The proliferation of devices that operate in the MMW range has been accompanied by increased concern about their safety. As MMW irradiation has a very shallow penetration in tissue, the specific absorption rate is not a relevant parameter for dosimetry purposes. A thermal modeling program was used to investigate the tissue heating effects of MMW irradiation (100 GHz nominal) on the primate head. The objectives were to determine the extent to which the surface and subsurface tissue temperatures depend on applied energy density and the effects of blood flow and surface cooling on tissue temperatures. Two power ranges were considered: short-duration exposure to high-power microwaves (HPMs), with power densities of 1.0, 1.5, 2.0, 2.5, or 3.0 W $\cdot$ cm^{-2} for 3 s, and longer duration exposure to low-power microwaves (LPMs), with power densities of 0.1, 0.15, 0.2, 0.25, 0.3 W $\cdot$ cm^{-2} for 30 s. The applied energies were comparable for both HPM and LPM exposures. We found both surface and subsurface temperatures increase as the energy level increases, with HPMs having a higher peak temperature than the LPMs for similar exposure energy densities. The surface temperature increase is linear with energy density for the HPMs, except under combined conditions of high blood flow (blood-flow rate of 8×10^{-3} g $\cdot$ s^{-1} $\cdot$ cm^{-3}) and high-energy density (greater than 7.5 J $\cdot$ cm^{-2}). The LPM surface temperatures are not linear with incident energy. The peak surface temperature is affected by environmental conditions (convection coefficient, sweat rate.) The magnitude of the temperature increase due to MMW exposure did not change with environmental conditions. The subsurface temperature increases are considerably damped, compared to the surface temperatures.**

NOMENCLATURE

c	Specific heat (J $\cdot$ g^{-1} $\cdot$ °C^{-1}.
f	Frequency (MHz).
h	Convective heat transfer coefficient (W $\cdot$ cm^{-2} $\cdot$ °C^{-1}).
i_{fs}	Specific enthalpy of vaporization of water (J $\cdot$ g^{-1}).
k	Thermal conductivity (W $\cdot$ cm^{-1} $\cdot$ °C^{-1}).
L	Thermal diffusion length scale (cm).
$\dot{m}_b$	Mass flow rate of blood, per unit tissue volume (g $\cdot$ s^{-1} $\cdot$ cm^3).
$\dot{m}_{\rm evap}$	Rate of water evaporation, per unit surface area (g $\cdot$ cm^{-2} $\cdot$ s^{-1}).
$\vec{n}$	Surface normal vector.
$\dot{q}_m$	Metabolic heat rate (W $\cdot$ cm^{-3}).
$\vec{q}''_{\rm MMW}$	Power density vector for millimeter-wave irradiation (W $\cdot$ cm^{-2}).
$q''_{\rm surf}$	Surface heat flux rate (W $\cdot$ cm^{-2}).
T	Temperature (°C).
α	Thermal diffusivity (cm^2 $\cdot$ s^{-1}).
δ	Penetration depth (cm).
ε'	Real part of the complex relative permittivity (dielectric constant).
ε''	Imaginary part of the complex relative permittivity (dielectric constant).
ρ	Mass density (g $\cdot$ cm^{-3}).
τ	Thermal diffusion time (s).

A. Subscripts

amb	Ambient.
art	Arterial.
b	Blood.
surf	Skin surface.
t	Tissue.
w	Water.

I. INTRODUCTION

MILLIMETER microwaves (MMWs) are a subset of the RF portion of the electromagnetic spectrum, comprising the 30–300-GHz range. Devices using MMWs include automobile collision avoidance systems [1], [2], medical applications, wireless communications systems [3], [4], and military devices [3].

The principal biological effect of MMW exposure is heating of superficial tissue. In this respect, the effects are qualitatively similar to the effects of exposure to IR energy [5], although the depth of penetration is somewhat greater for MMW than for IR irradiation. The greater penetration depth of MMW (compared to IR exposure) may imply significant differences in the sensory response to similar energies of IR and MMW exposure. At longer wavelengths, this may result in a risk of absorbing dangerous levels of energy before an avoidance response is stimulated [6].

Historically, RF exposure standards have been based on limiting the specific absorption rate (SAR). Maximum permissible exposure (MPE) levels are based on a nominal safe exposure criterion SAR $\leq$0.4 W/kg in the frequency range 0.1 MHz $< f <$ 6.0 GHz. At higher frequencies (which includes most of the MMW band), "... the exposures are quasi-optical, and ... power density is the meaningful parameter" [7].

Manuscript received November 29, 1999; revised March 1, 2000. This work was sponsored by the U.S. Air Force.

D. A. Nelson is with the Center for Biomedical Engineering, Michigan Technological University, Houghton, MI 49931 USA and also with the Radio Frequency Radiation Branch, Air Force Research Laboratory, Brooks Air Force Base, TX 78235 USA.

M. T. Nelson is with the Center for Biomedical Engineering, Michigan Technological University, Houghton, MI 49931 USA.

T. J. Walters is with Veridian Engineering, San Antonio, TX 78235 USA.

P. A. Mason is with Conceptual MindWorks, Inc., San Antonio TX 78235.

Publisher Item Identifier S 0018-9480(00)09704-0.

The IEEE recently adopted revised standards for human exposure to RF fields, specifying MPE levels for millimeter-wave irradiation. For MMW exposures in controlled environments, the whole-body MPE in terms of power density is 10 mW · cm^{-2}, based on an averaging time of between 10 s–6 min (depending on frequency.) For partial-body exposures, the standard allows a local time-averaged power density as high as 40 mW · cm^2 over similar averaging times [7].

For short-duration pulse exposures, (i.e., where the pulse duration is less than the specified averaging time), the allowable peak transient power density may be considerably higher than the corresponding time-averaged value [7].

As MMW irradiation does not penetrate very far into the skin (less than 0.5 mm at 100 GHz), the primary effect of exposure is surface heating [8]. The local temperature rise potentially is affected by heat conduction to surrounding tissue, advection (blood flow), surface convection [9], and perhaps other thermoregulatory responses (e.g., sweating, pilo-erection). This may make it difficult to predict thermal hazards on the basis of power density alone, and complicates the use of animal models to predict risk to humans.

A realistic three-dimensional (3-D) model that could accurately predict temperature distributions with a high degree of spatial resolution in bodies exposed to electromagnetic radiation would be excellent for the development of therapeutic applications, the determination of the potential harmful effects of MMW irradiation, and establishing safety standards [10], [11]. In addition, an accurate model is useful in extrapolating animal results to humans.

Extrapolation of experimental results from animal models to humans may be complicated by species differences in thermal dissipation mechanisms, notably evaporative cooling. Nonhuman primate species vary in their ability to sweat; otherwise their thermoregulatory systems are similar to a human's system [12]. Extrapolation of nonhuman primate experimental results to humans requires quantification of the significance of sweating (or the absence of the ability to sweat) in the cooling of the nonhuman primate subjected to MMW irradiation.

Our hypotheses are: 1) temperatures at and near the surface increase under MMW exposure; 2) surface temperature increase is approximately linear with applied energy density; 3) surface temperature is depressed under conditions of increased surface cooling (i.e., higher convection coefficient and/or sweat rate); 4) temperature below the scalp surface lags surface temperature and the magnitude of the temperature increase is diminished compared to the surface; and 5) deep and cranial temperatures (e.g., brain) are not affected by MMW exposure.

The goal of this paper is to develop a realistic model of the thermal effects (surface and subsurface) of millimeter-wave exposure in the primate (monkey) head, and use the model to test our hypotheses. This model would account for surface heating due to high power microwaves (HPMs) and low power microwaves (LPMs), and also the effects of surface convection, surface sweating, blood flow, and metabolic heating. The model would be heterogeneous, with four layers: the brain, cerebrospinal fluid (CSF), skull, and scalp. The energy deposition pattern would be the same for both the HPM and LPM, but the power density and time that the transmitter would be turned on would be different. For a given power deposition pattern, tissue properties (thermal conductivity, thermal diffusivity, and perfusion, or blood flow) are the major determinants of the resultant temperature field [13].

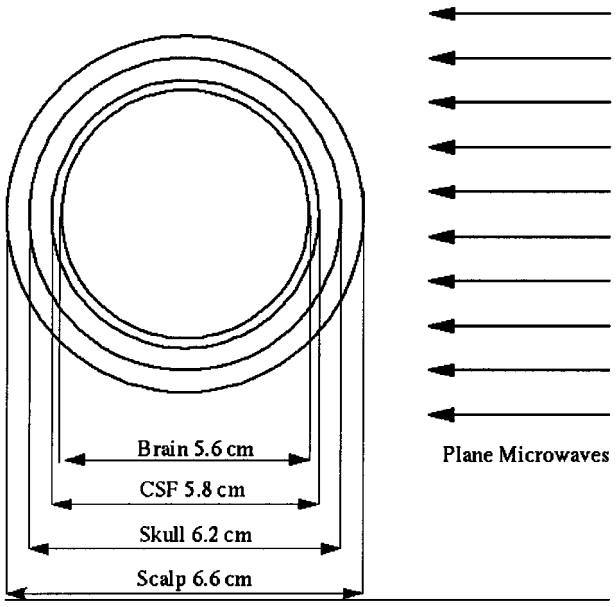

Fig. 1. Physical situation described by the model: plane wave microwaves irradiating a cranial model composed of four layers.

II. Methods

We created a spherical heterogeneous model to simulate the heating effects on a primate (monkey) head exposed to far-field radiation at 100 GHz (nominal). We modeled the head as a sphere with a diameter of 6.6 cm (Fig. 1), consisting of four different tissue layers: the brain (outer diameter $= 5.6$ cm), CSF (outer diameter $= 5.8$ cm), skull (outer diameter $= 6.2$ cm), and the scalp (outer diameter $= 6.6$ cm) [14]. We investigated three different blood-flow values for the scalp: basal, represented by 8×10^{-4} g · s^{-1} · cm^{-3} (grams of blood per second per cm^3 of tissue),[1] vasodilated (8×10^{-3} g · s^{-1} · cm^{-3}), and a high flow rate (8×10^{-2} g · s^{-1} · cm^{-3}) [15]. Only the blood perfusion rate in the scalp layer (the outer 0.2 cm of the model) would change to dissipate heat, thus, the values for the blood perfusion rate in the brain and skull were held constant. (There is zero blood flow to the CSF layer.) Other property data were obtained from the literature [16]–[20], with values as listed in Table I.

A. Heat-Transfer Model

Temperature calculations were based on a discretized version of the Pennes bio-heat transfer equation [21]

$$k_t \nabla^2 T + \dot{m}_b c_b (T_{\text{art}} - T) + \dot{q}_m = \rho_t c_t \frac{\partial T}{\partial t} \qquad (1)$$

where the deep arterial temperature $T_{\text{art}} = 38\ ^\circ\text{C}$ [22].

[1]The value for 8×10^{-4} g/s/cm^3 (grams of blood per second per cm^3 of tissue) is equivalent to 5 g/100 mL/min (grams of blood per 100-mL tissue per minute).

TABLE I
TISSUE THERMAL PROPERTY DATA

Tissue layer; Radius (cm)	Thermal conductivity ($W \cdot cm^{-1} \cdot °C^{-1}$)	Specific heat ($J \cdot g^{-1} \cdot °C^{-1}$)	Basal blood flow rate ($g \cdot s^{-1} \cdot cm^{-3}$)	Metabolic heat production ($W \cdot cm^{-3}$)
Brain; R =2.8	5.03×10^{-3}	3.5929	9.0×10^{-3}	.0110
CSF; R =2.9	6.37×10^{-3}	4.1790	0	0
Skull; R =3.1	4.99×10^{-3}	2.9719	3.0×10^{-4}	2.61×10^{-5}
Scalp; R =3.3	3.7×10^{-3}	3.700	8.0×10^{-4}	1.72×10^{-4}

We used the Thermal Analysis System (TAS) version 3.0.0 (Harvard Thermal Inc., Harvard MA) to calculate the temperatures at different locations within the sphere under various environmental conditions and thermal loads. The TAS program is a 3-D finite-difference-based program for evaluating conduction heat-transfer problems. The Gauss–Seidel method was used to obtain the results, with the relative convergence criterion set to 1×10^{-3}.

B. Penetration Depth

A characteristic of MMW irradiation is short penetration depth in tissue. The penetration depth is the distance into the tissue at which the E- and H-fields have decayed to $1/e(= 0.368)$ of their respective values at the surface, and the magnitude of the Poynting vector has decayed to $1/e^2$ of its surface value. The penetration depth, i.e., δ, is given by [8]

$$\delta = (67.52/f)\left[\sqrt{(\varepsilon')^2 + (\varepsilon'')^2} - \varepsilon'\right]^{-(1/2)} \quad (2)$$

where f is the frequency (in megahertz) and ε' and ε'' are the real and imaginary parts of the complex relative permittivity. Penetration depth δ increases with wavelength. From (2), the calculated penetration depth into 2/3 muscle tissue equivalent material (TEM) at 100 GHz is 0.036 cm.

As the penetration depth of MMW irradiation is extremely shallow, we modeled the heat loads as surface heat loads. We applied surface heating based on the incident power density per unit projected surface area in the plane of the beam. Maximum power per unit of surface area occurs when the surface normal is perpendicular to the E- and H-field vectors [8]. The hemisphere away from the transmitter is not directly heated by the microwaves (Fig. 1), thus, the nonirradiated side does not have any MMW surface heat loads. We assumed 100% energy absorption, consistent with Walters *et al.* [23], who determined the transmission coefficient is greater than 0.9 at 94 GHz.

C. Surface Heating/Cooling

The net heat flux at the skin surface q''_{surf} is the sum of the MMW absorption, the latent heat loss due to sweat evaporation, and the sensible heat loss due to convection to ambient

$$q''_{\text{surf}} = \vec{q}''_{\text{MMW}} \cdot \vec{n} - \dot{m}_{\text{evap}} \rho_w i_{fs} - h(T_{\text{surf}} - T_{\text{amb}}) \quad (3)$$

where $\vec{q}''_{\text{MMW}}$ is the MMW power density vector (i.e., Poynting vector) and $\vec{n}$ is the unit surface normal vector.

The quantity $\dot{m}_{\text{evap}}$ represents the rate of sweat evaporation, per unit surface area. This is not necessarily the same as the sweat secretion rate. In cases where the sweat secretion rate exceeds the evaporation rate (due to either profuse sweating, or high ambient humidity), beading sweat on the skin surface would likely affect the power absorption.

We chose the values for the sweat evaporation rate to simulate a moderate sweat rate in humans, equal to 2.5×10^{-5} L $\cdot$ $cm^{-2} \cdot h^{-1}$ [24]. The sweating described by this term is not a response to the MMW irradiation. While prolonged MMW exposure could induce increased sweating, no attempt was made to incorporate active thermoregulatory control in the model.

While some species of monkeys have the ability to sweat, the rates tend to be less than for humans under similar conditions [25]. In the event moderate sweating significantly affects the temperature response to MMW irradiation, it would suggest temperature results should be adjusted for sweat rate in extrapolating temperature response data from nonhuman primates to man.

The convection coefficient values used ($h = 5 \times 10^{-4} \cdot cm^{-2} \cdot °C^{-1}$, $h = 1 \times 10^{-3}$ W $\cdot$ $cm^{-2} \cdot °C^{-1}$, and $h = 5 \times 10^{-3}$ W $\cdot$ $cm^{-2} \cdot °C^{-1}$) span the range that would likely be encountered in a testing environment. The value of $h = 5 \times 10^{-4}$ W $\cdot$ $cm^{-2} \cdot °C^{-1}$ corresponds to natural convection (still air), i.e., the lowest anticipated value.

Tissue thermal properties, metabolic rates, and typical blood-flow rate data were obtained from the literature and are listed in Table I.

D. Initial Conditions

There are significant temperature differences between the brain and scalp, which may be affected by environmental conditions and surface cooling [14], [26]. We obtained estimates of steady-state tissue temperatures by evaluating the model under prescribed conditions with zero applied RF energy. The resulting steady-state temperatures were used as the initial conditions for the RF heating simulations.

III. RESULTS

We studied the temperature effects from changes in the following three variables:

1) surface convection coefficient;
2) surface evaporation rate (i.e., sweating);
3) blood-flow rate to the scalp/surface tissue.

We used two different microwave power ranges: HPMs with power densities of 1.0, 1.5, 2.0, 2.5, or 3.0 W $\cdot$ cm^{-2} for 3 s and LPMs with power densities of 0.1, 0.15, 0.2, 0.25, 0.3 W $\cdot$ cm^{-2} for 30 s. The applied energy densities (power density multiplied by exposure time) were comparable for the HPM and LPM exposures (3.0–9.0 J $\cdot$ cm^{-2}).

A. Blood-Flow Effects

1) Effects on skin surface temperature increases: The peak surface temperature increase is shown in Fig. 2 as a function of exposed energy density for various blood-flow rates. The peak surface temperature increase is the difference between the steady-state surface temperature (i.e., temperature prior to exposure) and the peak temperature at the surface during exposure.

We found little difference in the temperature increase for the blood perfusion rate of 8×10^{-4} g $\cdot$ s^{-1} $\cdot$ cm^{-3} compared with a perfusion rate of 8×10^{-3} g $\cdot$ s^{-1} $\cdot$ cm^{-3} (where 5 g $\cdot$

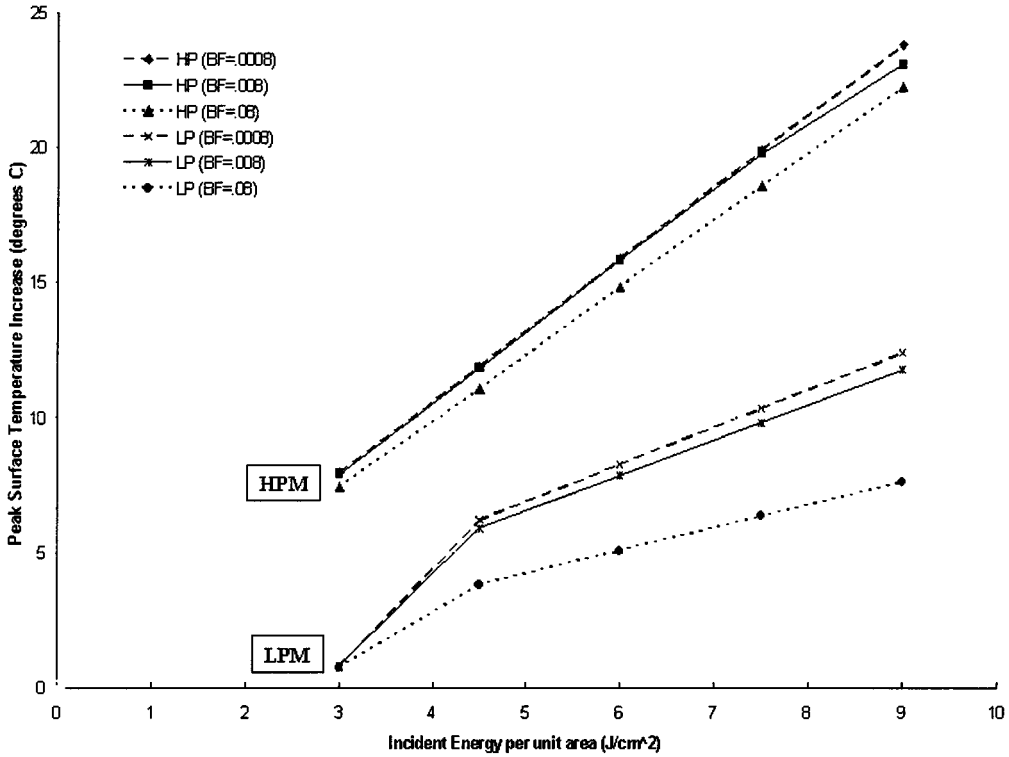

Fig. 2. Peak surface temperature increase (above steady-state surface temperature) versus applied energy density for three decades of tissue blood-flow rate (BF = blood-flow rate, in $g \cdot s^{-1} \cdot cm^{-3}$). Results are shown for an HPM ($1.0 - 3.0$ W $\cdot$ cm^{-2} for 3.0 s) and for an LPM (0.1–0.3 W $\cdot$ cm^{-2} for 30 s).

$(100\ mL)^{-1} \cdot min^{-1}$ is equivalent to 8×10^{-4} g $\cdot$ s^{-1} $\cdot$ cm^{-3}). When the blood perfusion rate was increased to 8×10^{-2} g $\cdot$ s^{-1} $\cdot$ cm^{-3}, the maximum temperature increase was reduced for both HPMs and LPMs. (The value of 8×10^{-2} g $\cdot$ s^{-1} $\cdot$ cm^{-3} was selected to determine the change in temperature under an extreme-high blood-flow rate, even though this value probably exceeds the physiologic range.)

The temperature increase was generally linear with applied energy density for HPMs (Fig. 2) with a divergence from linearity for a blood-flow rate of 8×10^{-3} g $\cdot$ s^{-1} $\cdot$ cm^{-3}, and an energy level above 7.5 J $\cdot$ cm^{-2}. The LPM peak temperature was linear with energy density for values greater than 4.5 J $\cdot$ cm^{-2} (Fig. 2).

2) Effects on surface and subsurface temperatures: While the maximum temperature effect is expected to occur at the surface, there may be significant temperature elevations in underlying tissues. Also, subsurface temperature trends are expected to lag the surface temperatures, both during and after exposure, i.e., we expected the subsurface tissue to heat and cool more slowly than the surface temperature.

Figs. 3 and 4 show the effects of increased scalp blood flow on tissue temperatures. These figures show the predicted temperature, rather than temperature increase above steady-state levels. Thus, the reported temperatures reflect the effects of environmental conditions on the initial (steady-state) temperatures, as well as the initial temperature gradient through the tissue layers.

We compared the LPM case of 0.1 W $\cdot$ cm^{-2} for 30 s (Fig. 3) and the HPM case of 1.0 W $\cdot$ cm^{-2} for 3 s (Fig. 4). For both HPM and LPM exposures, the convection coefficient was set to the still-air value of 5×10^{-4} W $\cdot$ cm^{-2} $\cdot$ °C^{-1} and the sweat rate was set to zero. Those conditions are considered a"worst case" since they would be expected to exhibit maximum sensitivity to changes in blood flow.

Fig. 3 shows the effect of blood flow on tissue temperatures for LPM exposure 0.1 W $\cdot$ cm^{-2}for 30 s). There was a slight difference (less than 0.5 °C) in the peak scalp surface temperatures observed with different blood-flow rates. For the basal blood-flow rate (8×10^{-4} g $\cdot$ s^{-1} $\cdot$ cm^{-3}), the peak surface ($R = 3.3$ cm) temperature was 40.6 °C [see Fig. 3(a)]. When we increased the blood-flow rate to the vasodilated level (8×10^{-3} g $\cdot$ s^{-1} $\cdot$ cm^{-3}), the peak surface temperature increased to 41.0 °C [see Fig. 3(b)]. With an extreme-high blood-flow rate (8×10^{-2} g $\cdot$ s^{-1} $\cdot$ cm^{-3}), the peak surface temperature decreased to 40.5 °C [see Fig. 3(c)]. The response of the next two interior temperatures in both cases was almost identical. The peak temperature in the mid-scalp ($R = 3.2$ cm) for the basal blood-flow rate was 39.0 °C [see Fig. 3(a)]. The other mid-scalp temperatures (blood-flow rates of 8×10^{-3} g $\cdot$ s^{-1} $\cdot$ cm^{-3} [see Fig. 3(b)] and 8×10^{-2} g $\cdot$ s^{-1} $\cdot$ cm^{-3} [see Fig. 3(c)]) were within 0.5 °C of each other.

The mid-skull peak temperature ($R = 3.0$ cm) was 37.8 °C for the basal blood-flow rate (8×10^{-4} g $\cdot$ s^{-1} $\cdot$ cm^{-3} [see Fig. 3(a)]). The other mid-skull temperatures (blood-flow rates of 8×10^{-3} g $\cdot$ s^{-1} $\cdot$ cm^{-3} [see Fig. 3(b)] and 8×10^{-2} g $\cdot$ s^{-1} $\cdot$ cm^{-3} [see Fig. 3(c)]) were within 0.5 °C of the value obtained under the basal blood-flow rate. Post-exposure temperatures dropped slightly faster with the extreme-high blood-flow rate, compared with the basal and vasodilated values (Fig. 3). The magnitude of the temperature increase was constant despite the change in the blood-flow rate.

Fig. 4 shows temperature versus time for HPM exposure of 1.0 W $\cdot$ cm^{-2} for 3 s, for three surface tissue blood-flow rates.

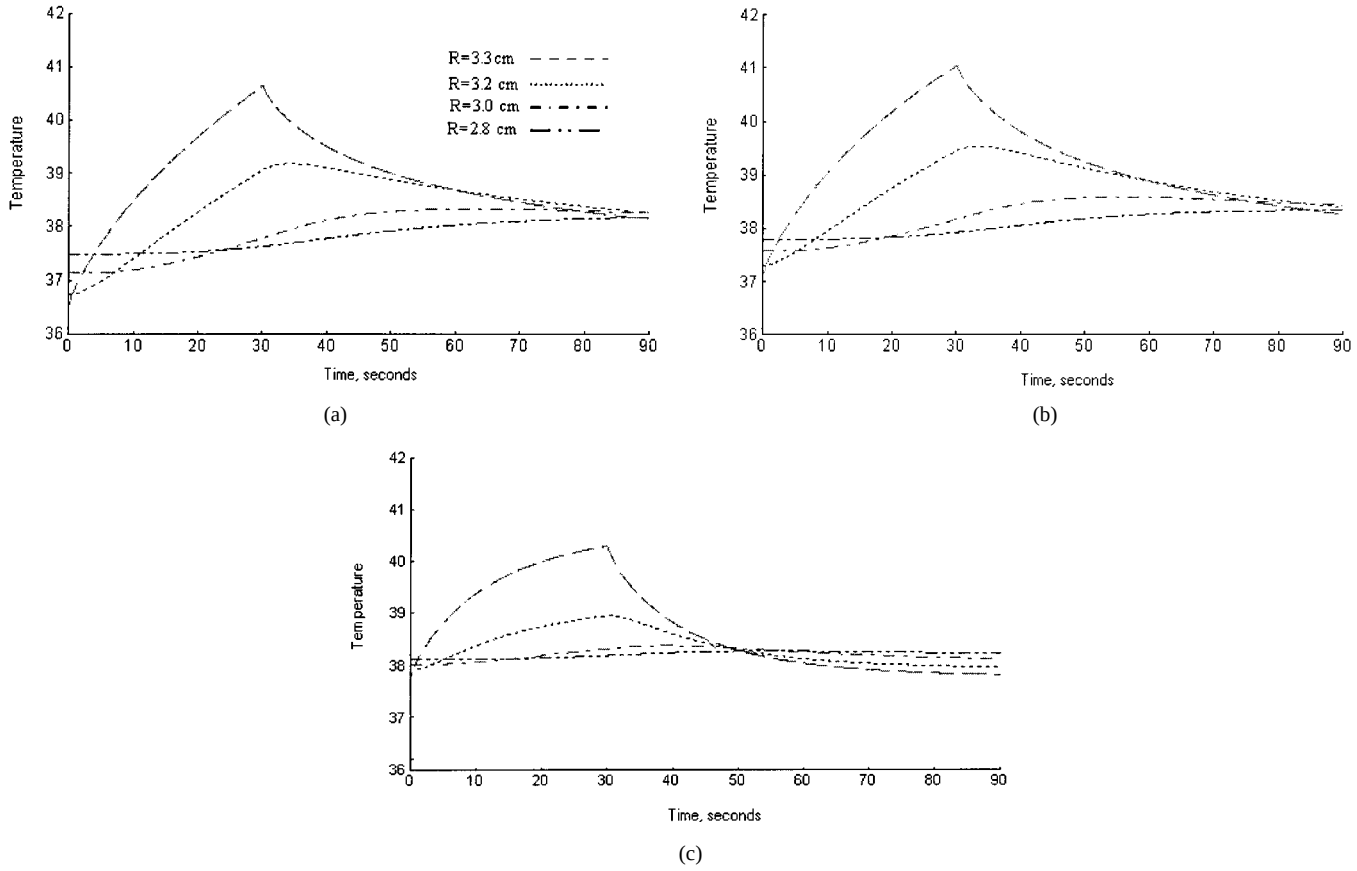

Fig. 3. Maximum surface and subsurface temperatures (in degrees Celsius) versus time (in seconds) for LPM (0.1 W · cm^{-2} for 30 s). (a) Tissue blood-flow rate $\dot{m}_b = 8 \times 10^{-4}$ g · s^{-1} · cm^{-3}. (b) $\dot{m}_b = 8 \times 10^{-3}$ g · s^{-1} · cm^{-3}. (c) $\dot{m}_b = 8 \times 10^{-2}$ g · s^{-1} · cm^{-3}. All three cases are for still air (20 °C; $h = 5 \times 10^{-4}$ W · cm^{-2} · °C^{-1}) and zero sweat evaporation rate.

The convection coefficient equals 5×10^{-4} W · cm^{-2} · °C^{-1} (still air; ambient temperature $= 20$ °C), and the sweat rate is zero for all three cases. The peak surface temperature increased slightly with increasing blood flow. There was a 0.5 °C increase in the peak surface temperature when the blood flow was increased from 8×10^{-4} g · s^{-1} · cm^{-3} [44.5 °C; see Fig. 4(a)] to 8×10^{-3} g · s^{-1} · cm^{-3} [45.0 °C; see Fig. 4(b)]. The extreme-high blood-flow rate (8×10^{-2} g · s^{-1} · cm^{-3} [see Fig. 4(c)]) produced a peak surface temperature of 45.2 °C.

This increase in surface temperatures with increasing blood-flow rate is due to the higher initial (steady-state) temperatures at higher flow rates. Increasing the blood flow from the basal rate (8×10^{-4} g · s^{-1} · cm^{-3}) to the middle (vasodilated) rate of 8×10^{-3} g · s^{-1} · cm^{-3} increased the steady-state surface temperature by 0.6 °C. At the extreme-high blood-flow rate (8×10^{-2} g · s^{-1} · cm^{-3}), the initial surface temperature was increased 1.3 °C over that for the basal blood-flow rate.

The temperatures at 1-mm subsurface, in the middle of the scalp tissue layer, were substantially depressed from the corresponding surface values. The mid-scalp ($R = 3.2$ cm) peak temperatures were 39.4 °C for both the basal blood-flow rate (8×10^{-4} g · s^{-1} · cm^{-3} [see Fig. 4(a)]) and the extreme-high blood-flow rate (8×10^{-2} g · s^{-1} · cm^{-3} [see Fig. 4(c)]). For the vasodilated blood-flow rate (8×10^{-3} g · s^{-1} · cm^{-3}) the mid-scalp peak temperature was 39.8 °C [see Fig. 4(b)].

Within the skull layer, the mid-skull peak temperature was 38.5 °C for all tissue blood-flow rates (Fig. 4).

B. Effects of Sweating

Fig. 5 shows the effect of sweating with LPMs at 0.1 W · cm^{-2} for 30 s with a convection coefficient of 5×10^{-4} W · cm^{-2} · °C. The peak scalp surface temperature [see Fig. 5(a)] was 3 °C cooler with a moderate sweat evaporation rate than with zero sweat evaporation. The mid-scalp peak temperature was 2.5 °C cooler with a moderate sweat evaporation rate [see Fig. 5(b)] compared to the nonsweating case [see Fig. 5(a)]. Sweating lowers the peak scalp temperature, but does not affect the magnitude of the temperature increase [see Fig. 5(b)] over pre-exposure levels.

Fig. 6 shows the effect of sweating on the temperature with HPM exposure of 1.0 W · cm^{-2} for 3 s with a convection coefficient of 5×10^{-4} W · cm^{-2} · °C^{-1}. When the sweat evaporation rate was increased from zero [see Fig. 6(a)] to a moderate sweat evaporation rate of 2.5×10^{-5} L · cm^{-2} · h^{-1} [see Fig. 6(b)] the peak scalp surface temperature decreased 3 °C. The mid-scalp peak temperature was about 3 °C cooler with a moderate sweat evaporation rate [see Fig. 6(b)] compared to the no sweating case [see Fig. 6(a)]). Moderate sweat evaporation results [see Fig. 6(b)] show the scalp surface, mid-scalp, and mid-skull peak temperatures were less than under nonsweating

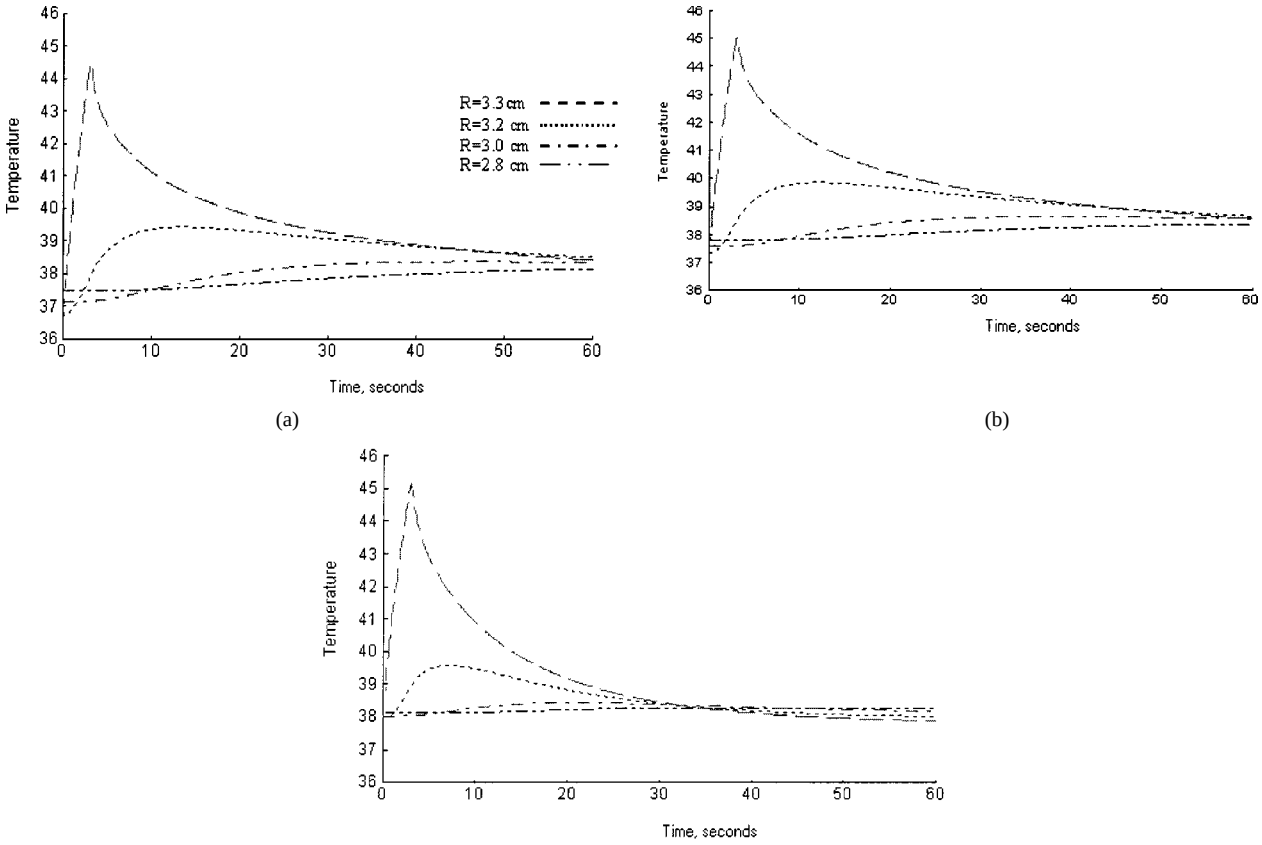

Fig. 4. Maximum surface and subsurface temperatures (in degrees Celsius) versus time (in seconds) for HPM (1.0 W $\cdot$ cm^{-2} for 3.0 s). (a) Tissue blood-flow rate $\dot{m}_b = 8 \times 10^{-4}$ g $\cdot$ s^{-1} $\cdot$ cm^{-3}. (b) $\dot{m}_b = 8 \times 10^{-3}$ g $\cdot$ s^{-1} $\cdot$ cm^{-3}. (c) $\dot{m}_b = 8 \times 10^{-2}$ g $\cdot$ s^{-1} $\cdot$ cm^{-3}. All three cases are for still air (20 °C; $h = 5 \times 10^{-4}$ W $\cdot$ cm^{-2} $\cdot$ °C^{-1}) and zero sweat evaporation rate.

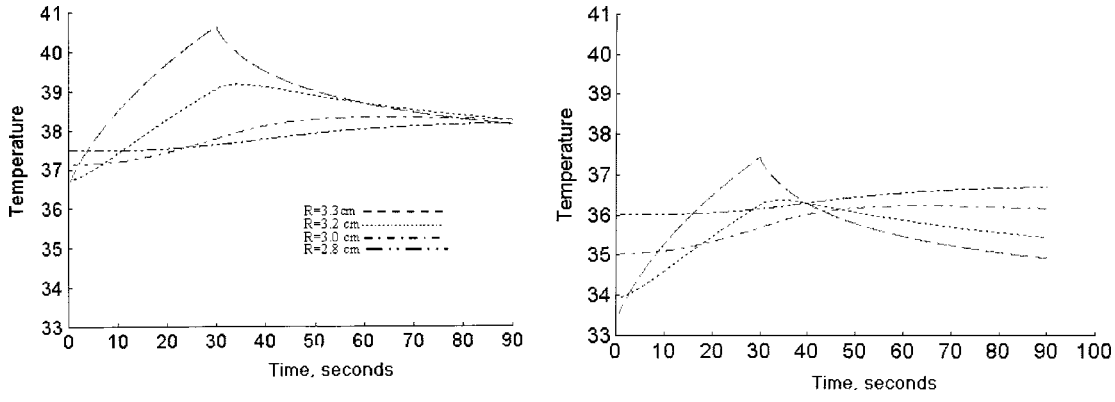

Fig. 5. Maximum surface and subsurface temperatures (in degrees Celsius) versus time (in seconds) for LPM (0.1 W $\cdot$ cm^{-2} for 30 s) in still air (20 °C; $h = 5 \times 10^{-4}$ W $\cdot$ cm^{-2} $\cdot$ °C^{-1}). (a) Zero sweat evaporation rate and (b) sweat evaporation rate of 2.5 $\times$ 10^{-5} L $\cdot$ cm^{-2} $\cdot$ h^{-1}.

conditions [see Fig. 6(a)], while the temperature at the brain surface ($R = 2.8$ cm) changed very little. The peak temperatures were affected by the sweating rate, but the temperature increase (the peak temperature minus the initial temperature) was not affected by sweating.

C. Effects of Convection

Fig. 7 shows the effects of a convection coefficient on LPMs at 0.1 W $\cdot$ cm^{-2} for 30 s with zero sweat evaporation and a basal blood-flow rate of 8 $\times$ 10^{-4} g $\cdot$ s^{-1} $\cdot$ cm^{-3}. The peak surface temperature with a moderate convection coefficient [see Fig. 7(b)] was about 1.5 °C cooler than under still-air conditions [see Fig. 7(a)]. For still air, the mid-scalp and mid-skull peak temperatures were 1 °C cooler than the peak surface temperature under identical conditions. For a moderate convection coefficient of 1 $\times$ 10^{-3} W $\cdot$ cm^{-2} $\cdot$ °C^{-1} [see Fig. 7(b)], the mid-scalp and mid-skull peak temperatures were 2 °C cooler than the peak surface temperatures under identical conditions.

Fig. 8 shows the effects of convection on HPMs at 1.0 W $\cdot$ cm^{-2} for 3 s with the sweat rate set at zero and a nominal blood-flow rate of 8 $\times$ 10^{-4} g $\cdot$ s^{-1} $\cdot$ cm^{-3}. The peak scalp

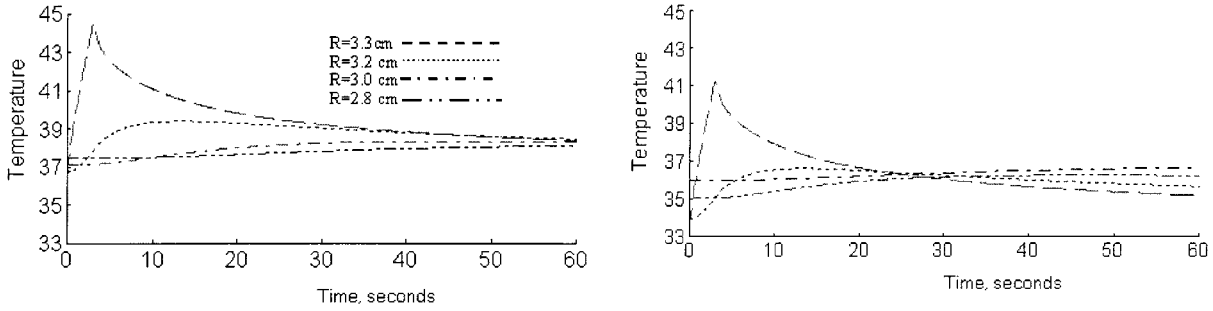

Fig. 6. Maximum surface and subsurface temperatures (in degrees Celsius) versus time (in seconds) for HPM (1.0 W $\cdot$ cm^{-2} for 3.0 s) in still air (20 °C; $h = 5 \times 10^{-4}$ W $\cdot$ cm^{-2} $\cdot$ °C^{-1}). : (a) Zero sweat evaporation rate and (b) sweat evaporation rate of 2.5×10^{-5} L $\cdot$ cm^{-2} $\cdot$ h^{-1}.

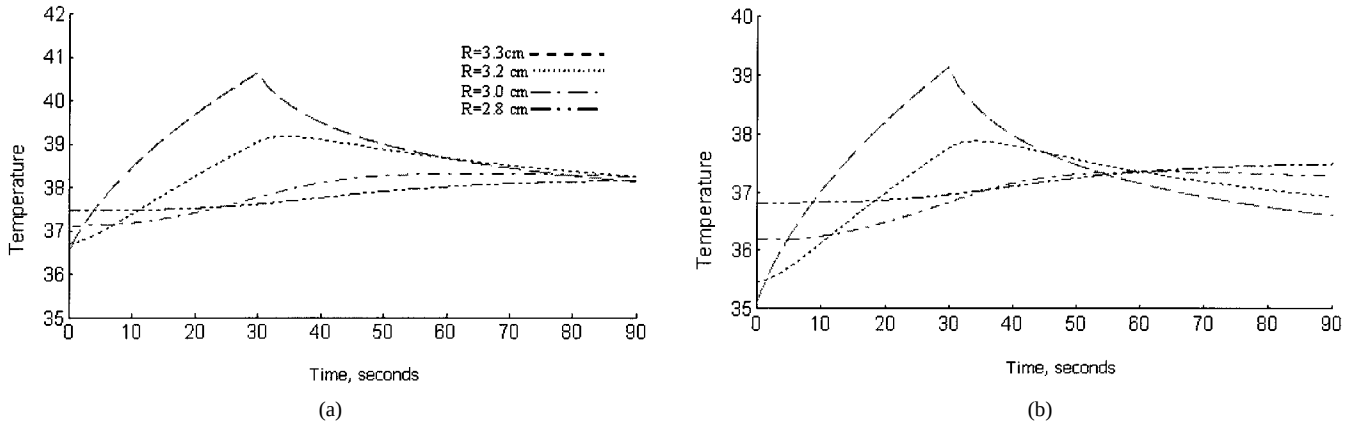

Fig. 7. Maximum surface temperature (in degrees Celsius) versus time (in seconds) for LPMs (0.1 W $\cdot$ cm^{-2} for 30 s). (a) Still air: $h = 5 \times 10^{-4}$ W $\cdot$ cm^{-2} $\cdot$ °C^{-1}. (b) Moderate convection coefficient: $h = 1 \times 10^{-3}$ W $\cdot$ cm^{-2} $\cdot$ °C^{-1}.

surface temperature with a moderate convection coefficient of 1.0×10^{-3} W $\cdot$ cm^{-2} $\cdot$ °C^{-1} [see Fig. 8(b)] was 1.5 °C cooler than the peak surface under still-air conditions (convection coefficient of 5×10^{-4} W $\cdot$ cm^{-2} $\cdot$ °C^{-1}). For the still-air conditions [see Fig. 8(a)], the peak temperatures in the mid-scalp and mid-skull were 5 °C cooler than the peak scalp surface temperature under identical conditions. For the moderate convection coefficient (1×10^{-3} W $\cdot$ cm^{-2} $\cdot$ °C^{-1} [see Fig. 8(b)]), the peak temperatures in the mid-scalp and mid-skull were 6 °C cooler than the peak scalp surface temperature under identical conditions.

When the convection coefficient was changed from a still air value, 5×10^{-4} W $\cdot$ cm^{-2} $\cdot$ °C^{-1} [see Fig. 8(a)] to a high value, 5×10^{-3} W $\cdot$ cm^{-2} $\cdot$ °C^{-1} [see Fig. 8(c)], peak surface temperature decreased 8 °C. For a high convection coefficient of 5×10^{-3} W $\cdot$ cm^{-2} $\cdot$ °C^{-1} [see Fig. 8(c)], the peak mid-scalp temperature was 7 °C cooler than the peak scalp surface. The peak mid-skull temperature was 6 °C cooler than the peak scalp surface temperature under identical conditions.

Despite the wide values of convection coefficients, the magnitude of the temperature increase did not change for either HPM or LPM exposures. However, the peak surface temperatures decreased as the convection coefficient increased due to lower initial (steady-state) temperatures at higher convection rates.

D. Metabolic Rate

Some species of monkeys may have a substantially higher metabolic rate than do humans [25]. We found that a fivefold increase in the metabolic rate did not affect the temperature increase. The difference between the temperature prior to exposure and the temperature during or subsequent to exposure was less than 0.01 °C.

It is also possible that prolonged exposure to RF irradiation may trigger a compensatory reduction in the metabolic rate. That scenario would be more likely under sustained whole-body irradiation, where the total thermal burden is significant and there is the possibility of elevation of body core temperature. Our results suggest superficial tissue temperatures, in the vicinity of localized MMW irradiation, are quite insensitive to metabolic rate.

E. MPE Effects

We investigated the effects of a 10 mW $\cdot$ cm^{-2} exposure for 30 s. This corresponds to the recommended MPE for controlled environments [7]. Under conditions of a basal blood-flow rate (8×10^{-4} g $\cdot$ s^{-1} $\cdot$ cm^{-3}), still air convection coefficient (5×10^{-4} W $\cdot$ cm^{-2} $\cdot$ °C^{-1}), and zero sweat rate, we found a peak temperature increase of less than 0.1 °C for a 30-s exposure.

IV. Discussion

A. Model Validation

Our model is consistent with the only known published results for skin surface temperature response to MMW irradiation. Walters *et al.* [23] showed a temperature increase of 7 °C for a MMW intensity of 1.05 W $\cdot$ cm^{-2} for 3 s at 94 GHz for

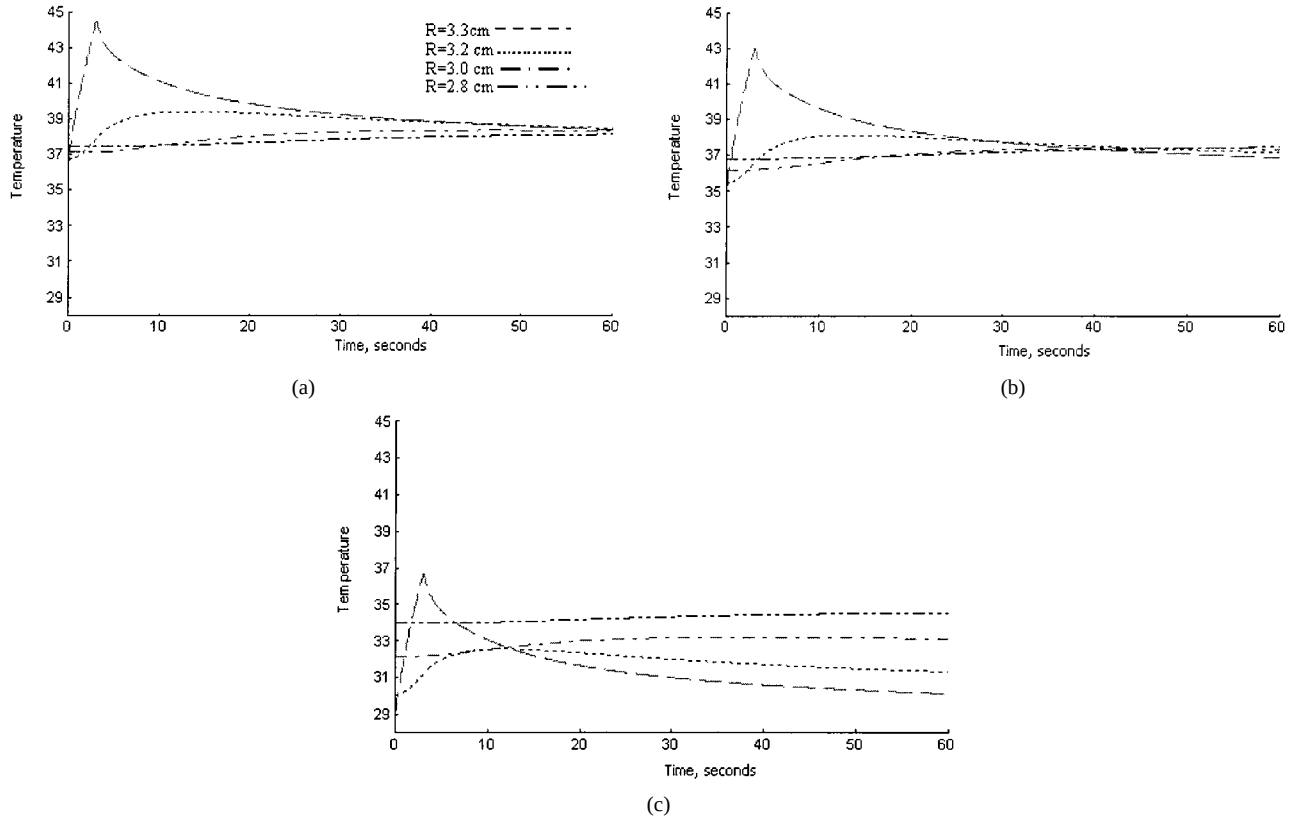

Fig. 8. Maximum surface and subsurface temperatures (in degrees Celsius) versus time (in seconds) for HPMs (1.0 W $\cdot$ cm^{-2} for 3.0 s). (a) Still air at 20 °C: $h = 5 \times 10^{-4}$ W $\cdot$ cm^{-2} $\cdot$ °C^{-1}. (b) Moderate convection coefficient: $h = 1 \times 10^{-3}$ W $\cdot$ cm^{-2} $\cdot$ °C^{-1}. (c) High convection coefficient: $h = 5 \times 10^{-3}$ W $\cdot$ cm^{-2} $\cdot$ °C^{-1}.

exposures on the human back. The peak surface temperature was 42.8 °C–43.8 °C, depending on the specific location on the human back. Under approximately the same environmental conditions (assumed convection coefficient of 5×10^{-3} W $\cdot$ cm^{-2} $\cdot$ °C^{-1}, sweating rate at zero, and blood-flow rate at 8×10^{-4} g $\cdot$ s^{-1} $\cdot$ cm^{-3}), the model results show a temperature increase of 8 °C (peak temperature of 44.5 °C).

B. Surface Temperature Increase

Surface temperature increases monotonically with energy density. However, the increase is less for LPMs than for HPMs for similar energy densities due to the longer time course of the LPM exposure. This allows time for the surface heat to be dissipated by convection, blood flow, sweating, and conduction.

The characteristic diffusion time τ can be estimated from the following: $\tau = L^2/\alpha$. Using a value for the thermal diffusivity of the scalp $\alpha = 1 \times 10^{-3}$ cm^2 $\cdot$ s^{-1} and $L = 0.1$ cm (the thickness of the outermost element) results in a characteristic thermal diffusion time $\tau = 10$ s. In the LPM case, energy is applied over a period of 30 s. A diffusion time of 10 s implies there would be significant diffusion of surface energy during the exposure interval. As the heating in the HPM case is only 3 s in duration, there is no significant conduction and, consequently, a greater increase in the surface temperature (Fig. 2).

The HPM temperature increase with respect to the energy density is linear, except under conditions of a blood-flow rate of 8×10^{-3} g $\cdot$ s^{-1} $\cdot$ cm^{-3} and an energy level above 7.5 J $\cdot$ cm^{-2}. The LPM temperature increase is linear above an energy level of 4.5 J $\cdot$ cm^{-2} (Fig. 2). Under conditions of either high blood-flow rates or slow heating, the rate of energy removal from the tissue volume due to advection or diffusion becomes significant relative to the rate of heating. The rate of surface temperature increase is, therefore, reduced.

C. Effects of Surface Cooling

The peak surface temperature is affected by various environmental conditions, but the magnitude of the temperature increase is not.

The surface and subsurface steady-state temperatures are decreased when the convection coefficient is increased from 5×10^{-4} W $\cdot$ cm^{-2} $\cdot$ °C^{-1} (simulating still air) to 5×10^{-3} W $\cdot$ cm^{-2} $\cdot$ °C^{-1} (simulating a light to moderate draft [see Fig. 8(a) and (c)]. Since the initial temperature is reduced, the peak temperature is reduced by the same magnitude.

The peak scalp surface temperature for LPM and HPM is 3 °C cooler when the sweat evaporation rate is 2.5×10^{-5} L $\cdot$ cm^{-2} $\cdot$ h^{-1} [see Figs. 5(b) and 6(b)] compared to no sweating [see Figs. 5(a) and 6(a)]. Sweating does affect the surface temperature for long exposures (30 s) and is a consideration when extrapolating data from monkeys to humans (Figs. 5 and 6). Sweating depresses the peak surface temperatures in both the LPM and HPM cases. Sweating can significantly depress the temperature of unexposed (nonirradiated) skin (i.e., the starting temperature is lower under moderate sweating than under nonsweating conditions) and causes the peak temperature to be less compared to the nonsweating condition. Since the peak surface

temperature is depressed due to sweating, it has implications for burn injury thresholds and pain sensation, which may depend upon skin surface temperature [23]. Therefore, sweating or lack thereof may alter exposure thresholds for burn injury and pain sensation.

Despite the change in the surface temperature depending on the convection coefficient or the sweat rate, the difference between the initial temperature and peak temperature showed little change.

D. Blood-Flow Effects

The effect of increased blood flow is to reduce the rate of temperature rise and cause a more rapid return to equilibrium temperature post-exposure (see Figs. 3 and 4). Increasing the blood flow tenfold over the basal rate increased the **steady state** surface temperature by 0.6 °C compared to the steady-state temperature for the basal blood-flow rate. However, the magnitude of the surface temperature **increase** during exposure did not change. Increasing the blood-flow rate further, by 100-fold over the basal rate increased the steady-state surface temperature by 1.3 °C compared to the steady-state temperature for the basal blood-flow rate. Again, the magnitude of the surface temperature **increase** did not change. At a high blood-flow rate of 8×10^{-2} g $\cdot$ s^{-1} $\cdot$ cm^{-3}, there is a decrease in the time lag (subsurface peak temperature lags surface peak temperature) at depths of 0.1 and 0.3 cm compared to the same depths with a nominal blood-flow rate of 8×10^{-4} g $\cdot$ s^{-1} $\cdot$ cm^{-3} (Figs. 3 and 4).

Our finding of a constant brain surface temperature, regardless of exposure conditions, is consistent with models of brain cooling in humans [14]. Cerebral temperatures are generally insensitive to surface conditions, and surface cooling affects only the most superficial brain tissue.

V. Conclusion

Temperature (surface and subsurface) increases as the energy level increases, with HPMs having a higher peak temperature than LPMs. The surface temperature increase is linear for the HPM surface temperatures with respect to the energy (Fig. 2), except for the HPM surface temperatures with a blood-flow rate of 8×10^{-3} g $\cdot$ s^{-1} $\cdot$ cm^{-3} and an energy level above 7.5 J $\cdot$ cm^{-2}. The LPM surface temperatures generally are not linear with energy density.

We found the peak surface temperature is affected by various environmental conditions (i.e., convection and sweat rate). However, the magnitude of the temperature **increase** due to MMW exposure did not change with environmental conditions. The mid-scalp and mid-skull temperature increases are less than, and lag the surface temperature. The subsurface temperatures are considerably damped compared to the scalp surface temperatures. We found that the brain surface temperature is constant for various environmental conditions, despite the wide variety of conditions applied to the scalp (Figs. 3–8). The results from our study also match well with the published experimental data [23].

A fivefold increase in the metabolic rate did not affect the magnitude of the temperature increase. The temperature difference between the baseline metabolic rate model and a high metabolic rate model (five times the baseline) was less than 0.01 °C.

Since the temperature increase did not change for various convection coefficients, sweat rates, blood-flow rates, and metabolic rates, physiological differences in thermoregulation between humans and nonhuman primates are not issues for predicting the temperature increase under MMW exposure. However, it is important in predicting the "actual" surface temperature.

It is not advisable to use a nonsweating primate as a model for human response under conditions where sweating might be induced since a moderate sweat rate (2.5×10^{-5} L $\cdot$ cm^{-2} $\cdot$ h^{-1}) will decrease the peak surface temperatures. A nonsweating primate is acceptable only for investigating the temperature difference between the peak exposure temperature and the initial (nonexposure) temperature since the magnitude of the temperature increase is the same with and without sweating.

Acknowledgment

The authors gratefully acknowledge the assistance and constructive comments of W. D. Hurt, Air Force Research Laboratory, Brooks AFB, TX, W. H. Cooke, Michigan Technological University, Houghton, MI, and B. H. Hamlin, Michigan Technological University, Houghton, MI, during the preparation of this paper's manuscript.

Trade names of materials and/or products of commercial or nongovernmental organizations are cited as needed for precision. These citations do not constitute official endorsement or approval of the use of such commercial materials and/or products.

References

[1] R. K. Gilbert, P. K. Zoratti, R. Becker, G. Brumbaugh, T. Chaplin, M. Harrison, M. Hawks, and K. Gondoly, "Characterization and evaluation of a prototype forward-looking automotive radar (FLAR) final report," ERIM Int. Inc., Ann Arbor, MI, Rep. DTNH22-94-Y-17 016, 1997.

[2] P. Moffa, J. Austin, G. S. Dow, I. Ikizyan, and M. Hibben, "Development of performance specifications for collision avoidance systems for lane change, merging, and backing—Task 5: Crash countermeasure technology investigation," TRW Space and Electron. Group, Redondo Beach, CA, DOT HS 808 506, 1996.

[3] K. L. Ryan, J. A. D'Andrea, J. R. Jauchem, and P. A. Mason, "Radio frequency radiation of millimeter wave length: Potential occupational safety issues related to surface heating," *Health Phys.*, vol. 78, pp. 170–181, 2000.

[4] A. G. Pakhomov, Y. Akyel, O. N. Pakhomova, B. E. Stuck, and M. R. Murphy, "Current state and implications of research on biological effects of millimeter waves," *Bioelectromagnetics*, vol. 19, pp. 393–413, 1998.

[5] E. R. Adair, "Infrared lasers & millimeter waves: The links between microwaves and laser optics," Air Force Research Lab., Brooks AFB, TX, AFRL-HE-BR-PC-1999-0002, 1999.

[6] D. W. Blick, E. R. Adair, W. D. Hurt, C. J. Sherry, T. J. Walters, and J. H. Merritt, "Thresholds of microwave-evoked warmth sensations in human skin," *Bioelectromagnetics*, vol. 18, pp. 403–409, 1997.

[7] *IEEE Standard for Safety Levels with Respect to Human Exposure to Radio Frequency Electromagnetic Fields, 3 kHz to 300 GHz*, IEEE Standard C95.119 99, 1999.

[8] C. H. Durney, H. Massoudi, and M. F. Iskander, *Radiofrequency Radiation Dosimetry Handbook*, 4th ed. Brooks AFB, TX: USAF School Aerospace Med., 1986.

[9] K. R. Foster, H. N. Kritikos, and H. P. Schwan, "Effect of surface cooling and blood flow on the microwave heating of tissue," *IEEE Trans. Biomed. Eng.*, vol. BME-25, pp. 313–316, May 1978.

[10] K. R. Foster, A. Lozano-Nieto, P. J. Riu, and T. S. Ely, "Heating of tissues by microwaves: A model analysis," *Bioelectromagnetics*, vol. 19, pp. 420–428, 1998.
[11] K. R. Foster and L. S. Erdreich, "Thermal models for microwave hazards and their role in standards development," *Bioelectromagnetics*, vol. 4, pp. 52–63, 1999.
[12] R. J. Spiegel, M. B. E. Fatami, and T. R. Ward, "A finite-difference electromagnetic deposition/thermoregulatory model: Comparison between theory and measurements," *Bioelectromagnetics*, vol. 8, pp. 259–273, 1987.
[13] W. H. Newman, P. P. Lee, and H. F. Bowman, "Limitations and significance of thermal washout data obtained during microwave and ultrasound hyperthermia," *Int. J. Hyperthermia*, vol. 6, pp. 771–784, 1990.
[14] D. A. Nelson and S. A. Nunneley, "Brain temperature and limits on transcranial cooling in humans: Quantitative modeling results," *European J. Appl. Physiol.*, vol. 78, pp. 353–359, 1998.
[15] W. M. Whelan, D. R. Wyman, and B. C. Wilson, "Investigations of large vessel cooling during interstitial laser heating," *Med. Phys.*, vol. 22, pp. 105–115, 1995.
[16] T. E. Cooper and G. J. Trezek, "Correlations of thermal properties of some human tissue with water content correlations of thermal properties of some human tissue with water content," *Aerospace Med.*, pp. 24–27, 1971.
[17] H. F. Bowman, E. G. Cravalho, and M. Woods, "Theory, measurement, and application of thermal properties of biomaterials," *Annu. Rev. Biophys. Bioeng.*, vol. 4, pp. 43–80, 1975.
[18] S. Vietla, R. C. Eberhart, and D. M. Meyer, "The influences of hypothermia and tissue perfusion on temperature distributions in simulated cranial surgery," in *Advances in Bioheat and Mass Transfer*. New York: Amer. Soc. Mech. Eng., 1993, vol. 268, pp. 9–17.
[19] A. Shitzer and R. C. Eberhart, "Heat generation, storage and transport processes," in *Heat Transfer in Medicine and Biology*. New York: Plenum, 1985, vol. 1, pp. 137–152.
[20] R. W. Olsen, L. J. Hayes, E. H. Wissler, H. Nikaidoh, and R. C. Eberhart, "Influence of hypothermia and circulatory arrest on cerebral temperature distributions," *J. Biomech. Eng.*, vol. 107, pp. 354–360, 1985.
[21] H. H. Pennes, "Analysis of tissue and arterial blood temperatures in the resting human forearm," *J. Appl. Physiol.*, vol. 1, pp. 93–122, 1948.
[22] M. A. Kolka and R. S. Elizondo, "Thermoregulation in *ereythrocebus patas*: A thermal balance study," *J. Appl. Physiol.*, vol. 55, pp. 1603–1608, 1983.
[23] T. J. Walters, D. W. Blick, L. R. Johnson, E. R. Adair, and K. R. Foster, "Heating and pain sensation produced in human skin by millimeter waves: Comparison to a simple thermal model," *Health Phys.*, vol. 78, pp. 259–267, 2000.
[24] S. K. Powers and E. T. Howley, "Exercise and the Environment," in *Exercise Physiology*, 4 ed. New York: McGraw-Hill, 2001, pp. 467–473, to be published.
[25] C. L. Heaps and S. H. Constable, "Physiological responses of rhesus monkeys to exercise at varied temperatures," *Aviat. Space Environ. Med.*, vol. 66, pp. 137–142, 1995.
[26] J. G. Stone, R. R. Goodman, H. Z. Baker, C. J. Baker, and R. A. Solomon, "Direct intraoperative measurement of human brain temperature," *Neurosurgery*, vol. 41, pp. 20–24, 1997.

D. A. Nelson, photograph and biography not available at time of publication.

M. T. Nelson, photograph and biography not available at time of publication.

T. J. Walters, photograph and biography not available at time of publication.

P. A. Mason, photograph and biography not available at time of publication.